Supplementary Material for

Interfacial engineering for redirecting CO_2 electroreduction selectivity on boron-doped diamond: from formic acid to carbon monoxide

Takashi Yamamoto,*[a] Taiga Ozawa,[a] Mai Tomisaki[b] and Yasuaki Einaga*[a]

[a]*Department of Chemistry, Keio University, Yokohama 223-8522, Japan.*

E-mail: takyama@chem.keio.ac.jp (T.Y.); einaga@keio.jp (Y.E.)

[b]*International Institute for Carbon-Neutral Energy Research (WPI-I2CNER), Kyushu University, Fukuoka 819-0395, Japan.*

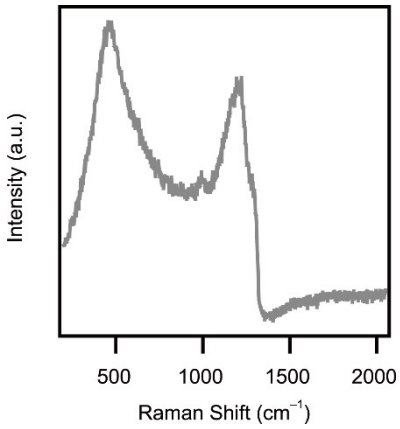

Fig. S1 A Raman spectrum of a boron-doped diamond (BDD) electrode.

Peaks at around 500 and 1200 cm^{-1} are attributed to the maxima of the phonon density of state of diamond. The peak at around 1330 cm^{-1} is attributed to the zone-center optical phonon of diamond.

[S1] S. Prawer, R. J. Nemanich, *Philos. Trans. R. Soc. A*, 2004, **362**, 2537−2565.

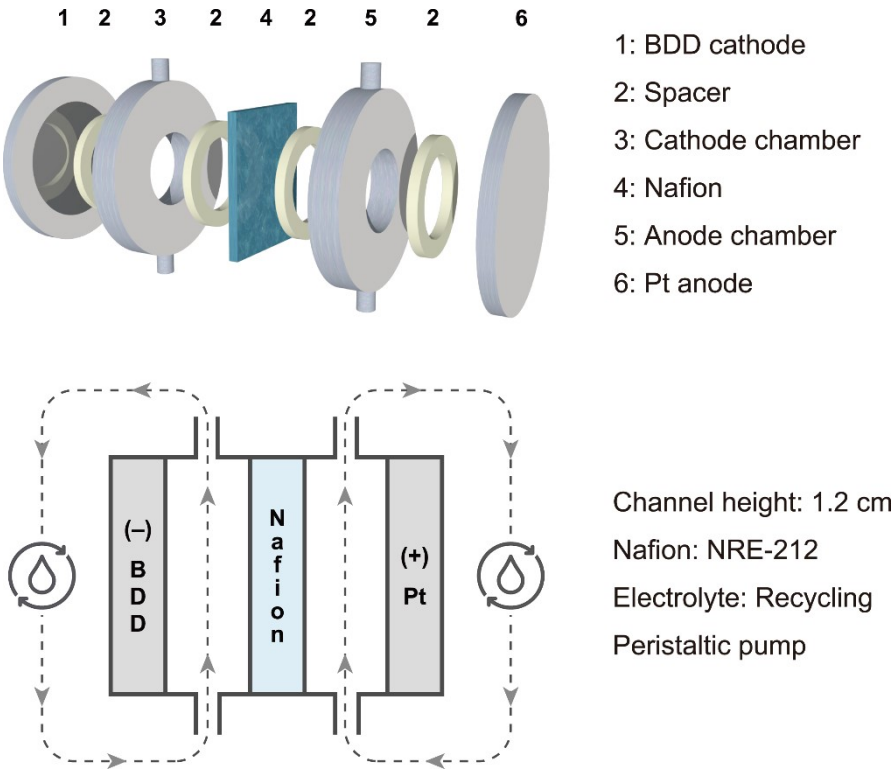

Fig. S2 A schematic illustration of the two-compartment PTFE flow cell.

The electrolyte was circulated using a peristaltic pump, with the flow direction indicated by the arrows in Fig. S2. Both the cathode and anode chambers are 1.2 cm thick. Electrical contact was ensured by attaching Cu plates to the rear surfaces of the BDD electrode and the Pt plate.

[S2] K. Natsui, H. Iwakawa, N. Ikemiya, K. Nakata, Y. Einaga, *Angew. Chem. Int. Ed.*, 2018, **57**, 2639–2643

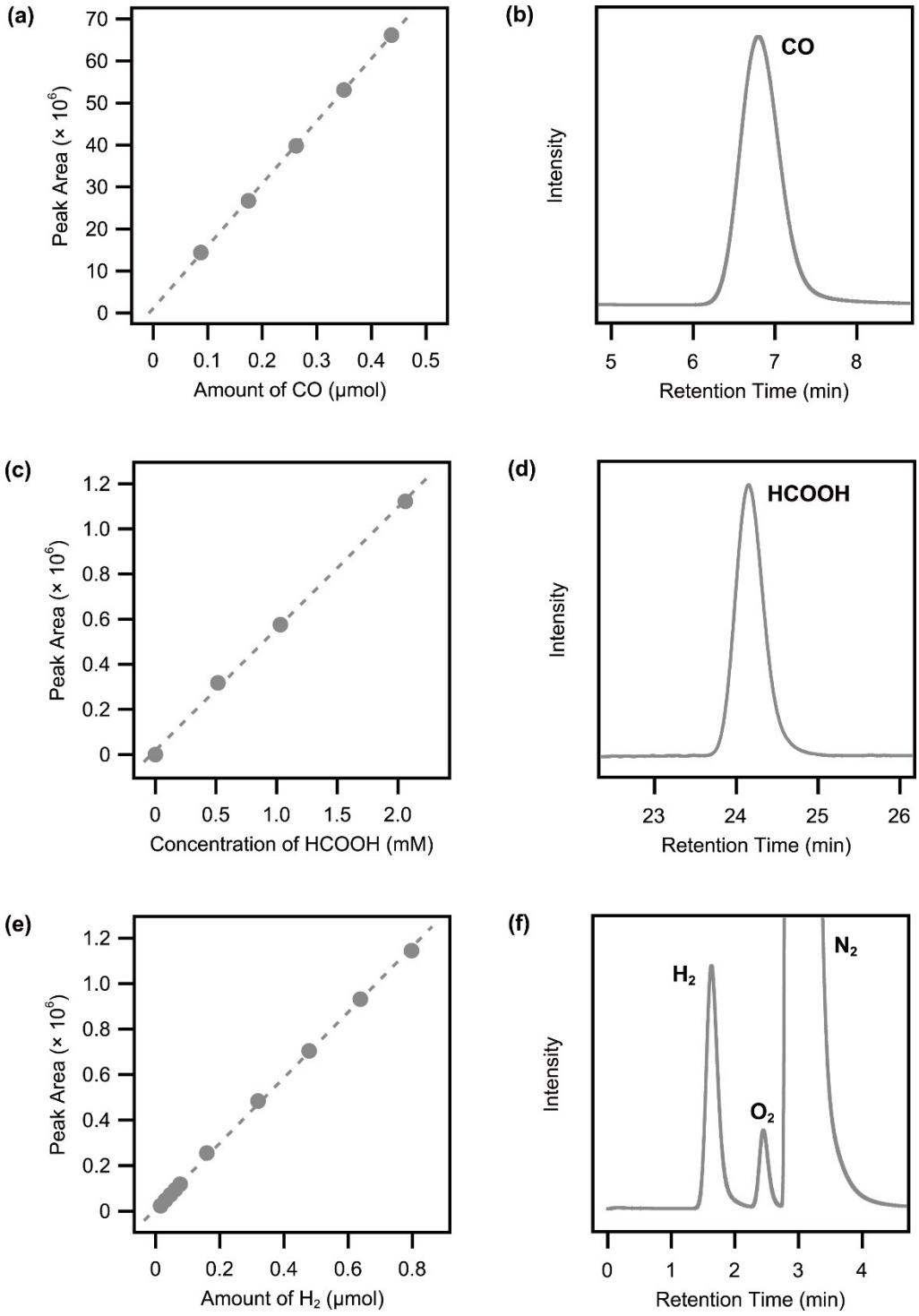

Fig. S3 Calibration curves and chromatograms. (a) The calibration curve for CO, (b) A gas chromatogram for CO, (c) The calibration curve for HCOOH, (d) A high-performance liquid chromatogram for HCOOH, (e) The calibration curve for H_2, and (f) A gas chromatogram for H_2. Measurements are performed with the GC and HPLC systems described in the Methods section.

Table S1 Detailed table of potential dependence on the eCO_2RR products. Conditions: 0.1 M $KClO_4$ aqueous solution, electrolyte flow rate of 100 mL min^{-1}, and operating temperature of 22 °C.

Potential (V *vs.* Ag/AgCl)	Potential (V *vs.* RHE)	j_{Total} [1] (mA cm^{-2})	j_{CO} [2] (mA cm^{-2})	Electrolysis Time (min)
−2.4	−1.96	−4.63	−0.45	24
−2.2	−1.76	−4.98	−0.65	24
−2.0	−1.56	−1.44	−0.72	73
−1.9	−1.46	−0.82	−0.49	128
−1.8	−1.36	−0.44	−0.23	73
−1.6	−1.16	−0.09	−0.03	671

[1] Total current density, and [2] partial current density of CO production.

Potential (V *vs.* Ag/AgCl)	Potential (V *vs.* RHE)	FE_{CO} [1] (%)	SD [2] (%)	FE_{HCOOH} [3] (%)	FE_{H2} [4] (%)
−2.4	−1.96	9	1.53	2	82
−2.2	−1.76	13	1.15	1	86
−2.0	−1.56	44	1.53	4	40
−1.9	−1.46	53	0.58	5	30
−1.8	−1.36	43	2.08	9	29
−1.6	−1.16	17	2.31	9	26

[1] Faradaic efficiency of CO production, and [2] standard deviation of FE_{CO}, [3] Faradaic efficiency of HCOOH production, and [4] Faradaic efficiency of H_2 production. n = 3 for all investigations.

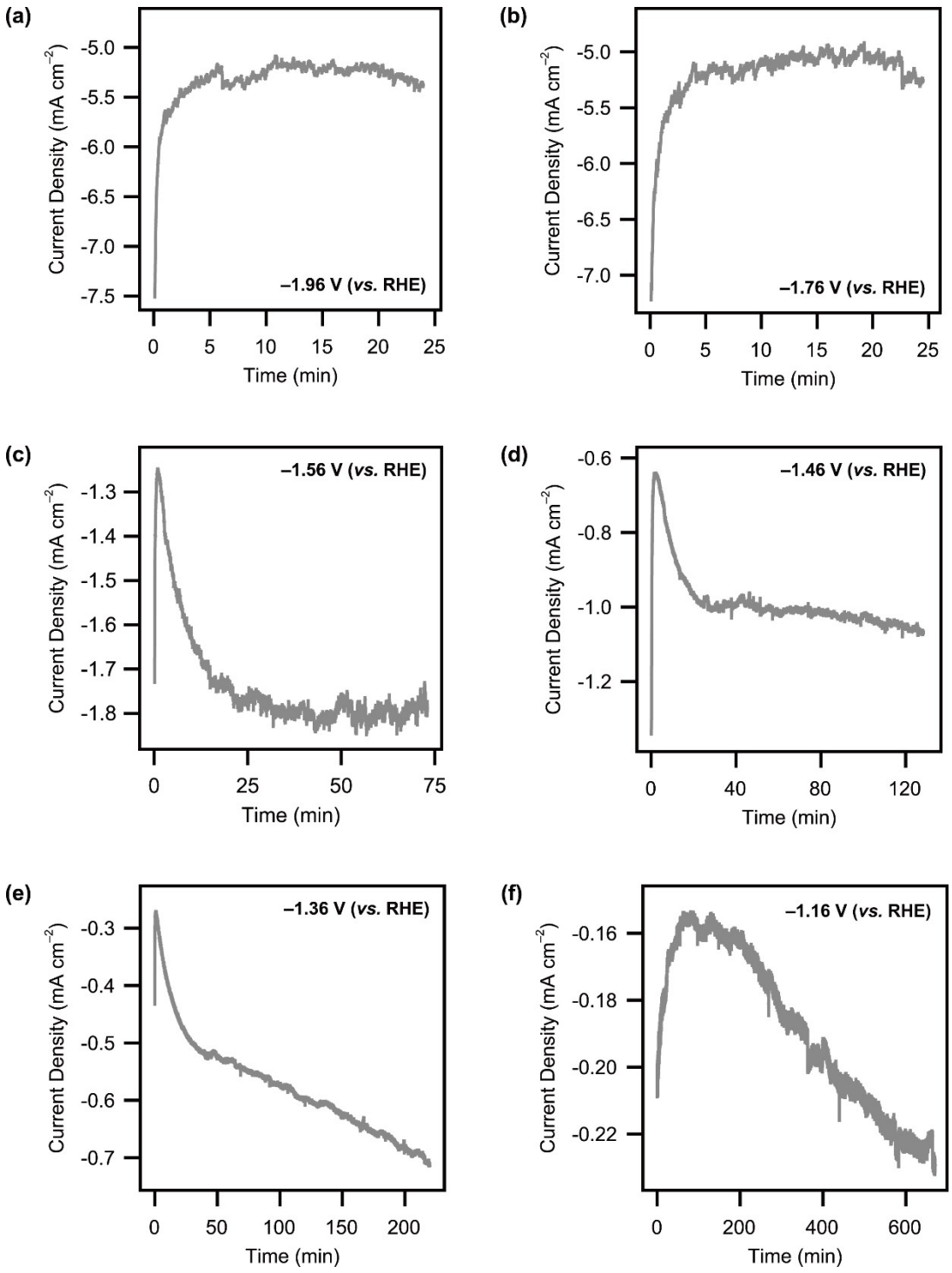

Fig. S4 Chronoamperograms during the eCO_2RR: (a) −1.96 V (*vs.* RHE), (b) −1.76 V (*vs.* RHE), (c) −1.56 V (*vs.* RHE), (d) −1.46 V (*vs.* RHE), (e) −1.36 V (*vs.* RHE), and (f) −1.16 V (*vs.* RHE). Other conditions: 0.1 M $KClO_4$ aqueous solution, electrolyte flow rate of 100 mL min^{-1}, and operating temperature of 22 °C.

Table S2 Detailed table of flow rate dependence on the eCO_2RR products. Conditions: applied potential of −1.46 V (*vs.* RHE), 0.1 M $KClO_4$ aqueous solution, and operating temperature of 22 °C.

Flow Rate (mL min^{-1})	j_{Total} [1] (mA cm^{-2})	j_{CO} [2] (mA cm^{-2})	Electrolysis Time (min)
100	−0.82	−0.49	128
200	−0.96	−0.62	116
300	−1.07	−0.71	106
400	−1.26	−0.90	92
500	−1.67	−1.20	71
600	−2.10	−1.42	58

[1] Total current density, and [2] partial current density of CO production.

Flow Rate (mL min^{-1})	FE_{CO} [1] (%)	SD [2] (%)	FE_{HCOOH} [3] (%)	FE_{H2} [4] (%)
100	53	0.58	5	30
200	60	2.65	10	23
300	63	1.73	15	17
400	69	2.08	17	11
500	71	1.15	16	12
600	69	1.53	28	5

[1] Faradaic efficiency of CO production, and [2] standard deviation of FE_{CO}, [3] Faradaic efficiency of HCOOH production, and [4] Faradaic efficiency of H_2 production. n = 3 for all investigations.

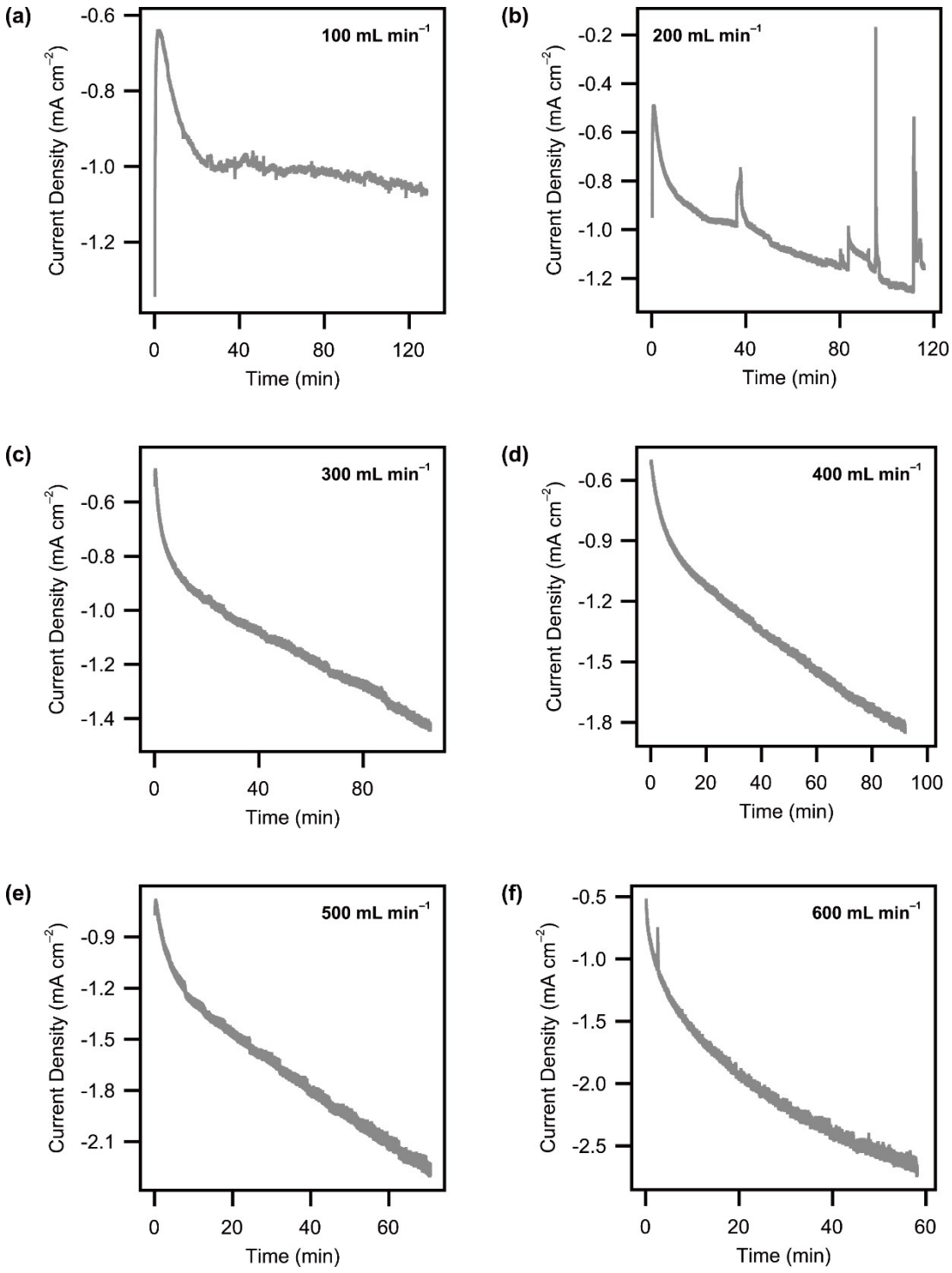

Fig. S5 Chronoamperograms during the eCO_2RR: (a) 100 mL min^{-1}, (b) 200 mL min^{-1}, (c) 300 mL min^{-1}, (d) 400 mL min^{-1}, (e) 500 mL min^{-1}, and (f) 600 mL min^{-1}. Other conditions: applied potential of −1.46 V (*vs.* RHE), 0.1 M $KClO_4$ aqueous solution, and operating temperature of 22 °C.

Table S3 Detailed table of temperature dependence on the eCO_2RR products. Conditions: applied potential of −1.46 V (*vs.* RHE), 0.1 M $KClO_4$ aqueous solution, and electrolyte flow rate of 500 mL min^{-1}.

Temperature (°C)	j_{Total} [1] (mA cm^{-2})	j_{CO} [2] (mA cm^{-2})	Electrolysis Time (min)
5	−1.37	−1.05	82
13	−1.39	−1.02	84
22	−1.63	−1.05	72
30	−2.23	−1.20	53

[1] Total current density, and [2] partial current density of CO production.

Temperature (°C)	FE_{CO} [1] (%)	SD [2] (%)	FE_{HCOOH} [3] (%)	FE_{H2} [4] (%)
5	72	0.58	14	8
13	72	1.53	15	11
22	63	1.73	12	23
30	53	2.08	14	32

[1] Faradaic efficiency of CO production, and [2] standard deviation of FE_{CO}, [3] Faradaic efficiency of HCOOH production, and [4] Faradaic efficiency of H_2 production. n = 3 for all investigations.

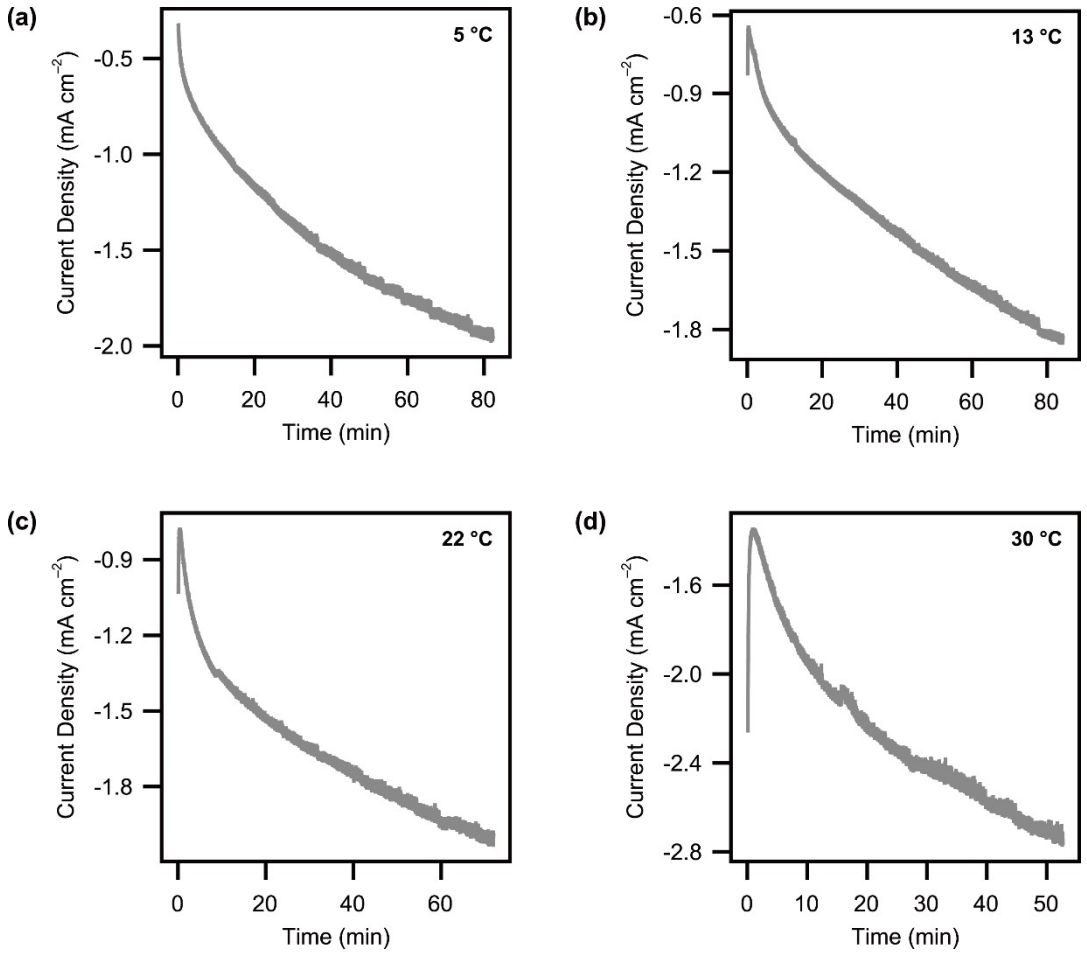

Fig. S6 Chronoamperograms during the eCO_2RR: (a) 5 °C, (b) 13 °C, (c) 22 °C, and (d) 30 °C. Other conditions: applied potential of −1.46 V (*vs.* RHE), 0.1 M $KClO_4$ aqueous solution, and electrolyte flow rate of 500 mL min^{-1}.

Table S4 Reproducibility of measurements of the diffusion layer thickness (δ) estimated from chronoamperometric measurements in 0.01 M $K_3[Fe(CN)_6]$ aqueous solution (pH 6.9) at −0.2 V (*vs.* Ag/AgCl) and 22 °C. The static condition (0 mL min^{-1}) is included for reference.

Flow Rate (mL min^{-1})	δ, Run 1 (μm)	δ, Run 2 (μm)	δ, Run 3 (μm)	Mean (μm)	SD [1] (μm)
0	714.3	725.2	718.0	719.2	5.543
100	134.9	128.8	141.4	135.0	6.301
200	91.79	102.6	94.70	96.37	5.594
300	78.26	70.49	82.22	76.99	5.972
400	75.07	71.67	64.11	70.28	5.610
500	69.48	72.44	62.39	68.10	5.164

[1] Standard deviation of δ.